PRODUCTION PROCESS

Investigation of the material combination 20MnCr5 and X45CrSi9-3 in the Tailored Forming of shafts with bearing seats

Laura Budde[1] · **Kai Biester**[1] · **Paulina Merkel**[2] · **Marius Lammers**[1] · **Mareile Kriwall**[2] · **Jörg Hermsdorf**[1] · **Malte Stonis**[2] · **Bernd-Arno Behrens**[2,3] · **Ludger Overmeyer**[1,4]

Abstract

The Tailored Forming process chain is used to manufacture hybrid components and consists of a joining process or Additive Manufacturing for various materials (e.g. deposition welding), subsequent hot forming, machining and heat treatment. In this way, components can be produced with materials adapted to the load case. For this paper, hybrid shafts are produced by deposition welding of a cladding made of X45CrSi9-3 onto a workpiece made from 20MnCr5. The hybrid shafts are then formed by means of cross-wedge rolling. It is investigated, how the thickness of the cladding and the type of cooling after hot forming (in air or in water) affect the properties of the cladding. The hybrid shafts are formed without layer separation. However, slight core loosening occurres in the area of the bearing seat due to the Mannesmann effect. The microhardness of the cladding is only slightly effected by the cooling strategy, while the microhardness of the base material is significantly higher in water cooled shafts. The microstructure of the cladding after both cooling strategies consists mainly of martensite. In the base material, air cooling results in a mainly ferritic microstructure with grains of ferrite-pearlite. Quenching in water results in a microstructure containing mainly martensite.

Keywords Laser hot-wire cladding · Cross-wedge rolling · Hybrid components · Cladding

1 Introduction

Components, e.g. shafts, must withstand various chemical, tribological and physical stresses during usage. During operation, some component areas are exposed to high mechanical loads. If the high stresses only occur in the area close to the surface, the use of a cost-intensive, high-strength material for the component can be avoided and the affected area can be cladded with a harder material, e.g. 100Cr6 or X45CrSi9-3, with a thickness of up to several millimeters instead. Various processes are available for applying these high-strength claddings. In order to achieve the final geometry, the cladding is subsequently machined. A disadvantage of cladding is the weld microstructure which is present in the cladding and in the heat-affected zone of the base material after the material is deposited. This can reduce the load capacity in the component area. Mildebrath et al. have demonstrated that the microstructure can be transformed into a fine-grained forming structure by subsequent hot forming [1].

2 State of the art

The combination of a joining process or Additive Manufacturing with a hot forming process, subsequent machining and, if necessary, heat treatment is known as a Tailored Forming process chain. The process chain is used for the production of hybrid components like axial bearing washers, bushings, shafts and bevel gears. Various material combinations were investigated for the production of Tailored

✉ Laura Budde
l.budde@lzh.de

1 Laser Zentrum Hannover e.V., Hollerithallee 8, 30419 Hannover, Germany

2 IPH-Institut für Integrierte Produktion Hannover gGmbH, Hollerithallee 6, 30419 Hannover, Germany

3 Institute of Forming Technology and Machines, Leibniz University Hannover, An der Universität 2, 30823 Garbsen, Germany

4 Institute of Transport and Automation Technology, Leibniz University Hannover, An der Universität 2, 30823 Garbsen, Germany

Forming components. The research results on the materials and process steps used in this investigation are presented in this section and the research question is derived.

2.1 Deposition welding

Various processes can be used for the production of claddings. The claddings can serve different purposes, such as corrosion or wear resistance. They are also used to improve surface hardness and strength. This is known as hardfacing. The layers can range from 0.5 mm to several millimeters in thickness [2]. Various processes are known for the welding of protective claddings. These processes are laser metal deposition with powder (LMD-P), laser hot-wire cladding (LHWC), laser induction cladding (LIC), gas metal arc welding (GMAW) or plasma transferred arc welding (PTA) [2–5].

The LHWC process is based on a laser beam and a hot-wire current source supplying energy to the process. The hot-wire current is used to heat the welding wire via resistive heating without melting the wire or igniting an electrical arc. In this state, the wire is melted by the laser beam in the process zone, causing it to pass into the melt pool [3, 4]. A large range of materials is available as cladding material for laser cold wire cladding (LCWC) and LHWC. For example steel, aluminum and titanium as well as stellite, nickel-based alloys and shape memory materials are usable materials [6].

By combining two energy sources, the laser beam and the hot-wire current source, the amount of heat can be fine-tuned and the laser power of a LHWC process can be reduced compared to the LCWC process with the same parameters. The wire feeding accuracy requirement decreases and the deposition welding efficiency can be increased. The hot-wire process influences the penetration depth and the microstructure while height and width of the weld seam are not affected [7–9].

2.2 Hot forming with the CWR process

Cross-wedge rolling (CWR) is a preform operation, that distributes masses on the workpiece prior to forging or milling, thereby increasing efficiency of subsequent processes. The quality of the rolled part in the Tailored Forming process chain depends, among others, on the process parameters of CWR forming. Important parameters are e.g. forming temperature, velocity, heating strategy and tool spacing. The surface of the tool has a pattern of forming wedges, that initiate the axial flow of material (see Fig. 1). Good process stability can be achieved when the cross-section reduction (dA) per forming wedge insertion is between 55 to 70%. When a higher dA is desired, then multiple wedges are used serially arranged to avoid necking, cracking or surface defects. The process stability is also influenced by the forming angle (α)
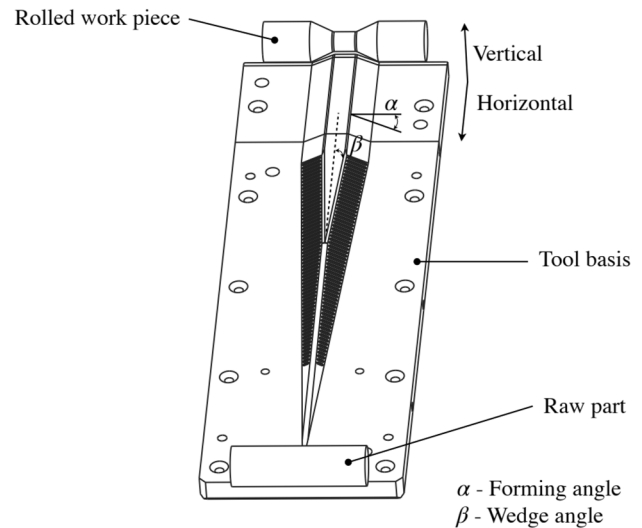

Fig. 1 The principle of material displacement during CWR, own figure according to [12]

and the wedge angle (β). For stable processes the parameters should be chosen according to Eqs. 1 and 2. [10–13]

$$15° \leq \alpha \leq 45° \tag{1}$$

$$3° \leq \beta \leq 15° \tag{2}$$

The CWR process has a strong influence on the microstructural properties of the workpiece. The grain size is related to the degree of forming and the rolling temperature. In areas where little forming occurs (e.g. in the bearing seat), the grain size remains similar to the grain size before forming. A higher degree of forming leads to the formation of smaller grains. At lower temperatures a mixed grain structure is formed, which has a negative effect on the mechanical properties of the workpiece. At high temperatures the grain size formed is finer. However, if the temperatures are too high, coarse grains are formed, which reduce the strength and plasticity of the workpiece [14, 15] .

Defects caused by CWR are the biggest challenge for industrial use. Common defects that occur are incomplete forming due to uncontrolled slipping, necking of the workpiece, surface defects and internal cracks. Internal cracks and voids are caused by the Mannesmann effect. This is a mechanism resulting from complex shear and tensile stresses in rolled workpieces, that creates internal voids. Internal voids significantly reduce the life of shafts and pose a major challenge. The mechanism of internal defects in a multi-wedge CWR-process is even more complicated, due to the complex stress conditions during forming. The most important factor influencing internal defects is the tool design. The probability of internal defects in the formed piece increases

with a lower forming angle α and a higher wedge angle β. The probability is additionally influenced by the amount of non-metallic inclusions, low material cohesion due to material fatigue, high temperatures and cyclically varying compressive and tensile stresses [10, 16–19].

2.3 Tailored forming process chain

The results of studies on the Tailored Forming process chain involving the materials or processes under investigation are presented in this section. Behrens et al. investigated the production of hybrid bevel gears [20]. A LHWC process was used to apply a cladding of X45CrSi9-3 on a base cylinder of mild steel. The hybrid semi-finished part was heated and die forged. A process-integrated heat treatment with a spray cooling system was performed after forging. After deposition welding a hardness of 380 to 400 HV0.5 was achieved in the cladding. A grain refinement in the cladding material and the base material was observed after hot forming. The cladding hardness after forging was dependent on the cooling strategy and the measurement area. Measurements were performed at the tooth root and the tooth tip at the lower part of the bevel gear (higher plastic strain during forming) and the upper part of the bevel gear (lower plastic strain during forming). Cladding hardness of bevel gears which were cooled at ambient air decreased to 279 HV0.5 at the lower part of the bevel gear. The hardness after heat treatment in the spray cooling system was increased to a range of 600 to 750 HV0.5. In the upper part of the bevel gear, the hardness after forging varied between 400 and 600 HV0.5. After heat treatment, a hardness of 600 to 850 HV0.5 was achieved.

Another forming process used in Tailored Forming is CWR. Kruse et al. investigated the cladding layer distribution after CWR of hybrid shafts with a base material of C22.8 and a cladding of X45CrSi9-3 and shafts with a base material of C22.8 and a cladding of 100Cr6 [5]. The shafts were successfully cross-wedge rolled without layer separation. The simulation results of the layer distribution were in good agreement with the experimental results. An initial cladding width of 15 mm after LHWC resulted in sufficient layer distribution in the area of the bearing seat, while the bearing seat was not completely covered when using cladding with a width of 8 mm.

In the aforementioned investigations, a cladding was applied circumferential to the shaft to produce the hybrid semi-finished product. This is particularly suitable for the production of shafts with bearing seats. However, it is also possible to reduce the cost and/or weight of the shaft by joining shafts made of two different materials in series. Blohm et al. investigated hybrid shafts of the material combination C22 and 20MnCr5 [21]. Two base cylinders with a diameter of 30 mm and a length of 50 mm were joined by laser deep welding and formed by CWR.

A reduction of cross-section during CWR of 19% and 72% was investigated. In both cases, no marks, necking and surface defects were visible after CWR. Kruse et al. extended those investigations towards hybrid shafts of the aluminium alloy EN AW 6082 and the steel 20MnCr5, which is particularly suitable for part weight optimization [13]. The base cylinders were joined by friction welding, and the displacement of the joining zone after CWR due to the diameter reduction in the area of the joining zone and axial movement of the shaft was determined by both experiment and simulation. The standard deviation of the joining zone displacement between simulation and experiment was 8.8%.

Previous studies on Tailored Forming of cladded semi finished parts have been limited to unalloyed mild steel like C22.8 as the base material. However, investigations of semi-finished products, which were manufactured by joining of two serially arranged base cylinders, have shown that the alloyed case-hardening steel 20MnCr5 could also be suitable for CWR. This material is used for components subject to alternating stresses, such as crown wheels, gears and shafts. This paper aims to investigate whether this material is also suitable for the production of hybrid components by cladding and CWR. Therefore, investigations on the use of 20MnCr5 as the base material and the high-strength X45CrSi9-3 as the cladding material are carried out.

The following research questions will be addressed in this paper:

1. Can hybrid components of the material combination X45CrSi9-3 and 20MnCr5 be successfully welded and cross-wedge rolled?
2. How are the layers distributed after welding and after cross-wedge rolling?
3. How does the cooling strategy affect the cladding and base material properties?
4. What hardness values can be achieved in the cladding and the base material?

3 Materials and methods

In this paper hybrid components of the materials combination 20MnCr5 and X45CrSi9-3 are manufactured using a LHWC process and a subsequent CWR process. Two different cooling strategies and their effect on the resulting cladding properties are investigated. The process steps and investigations are shown in Fig. 2.

Table 1 Chemical composition in wt.% of 20MnCr5 [22] and X45CrSi9-3 [23]

|	Fe	C	Si	Mn	P	S	Cr	Ni
20MnCr5 (1.7147)	Bal.	0.17–0.22	< 0.40	1.10–1.40		< 0.035	1.00–2.00	
X45CrSi9-3 (1.4718)	Bal.	0.40–0.50	2.70–3.30	< 0.60	< 0.04	< 0.030	8.00–10.00	< 0.50
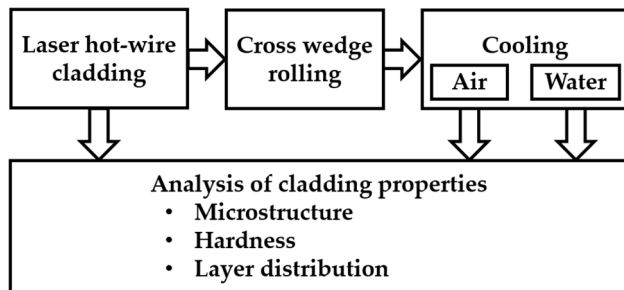
Fig. 2 Process steps and investigations

3.1 Materials

The base material used is the chrom-manganese alloyed case-hardening steel 20MnCr5. This steel is often used for gear parts. 20MnCr5 is considered weldable [22].

The martensitic chrom-silica steel X45CrSi9-3 is used as cladding material. The steel has good weldability. It also has good forming behavior and excellent surface hardenability. The material can have a hardness of > 57 HRC when quenched. The chemical composition of both materials is shown in Table 1 [23].

3.2 Experimental setup for laser hot-wire cladding

Claddings are applied on the base cylinder by LHWC. The experimental setup is shown in Fig. 3. The coaxial laser hot-wire deposition welding head MK-II, designed and manufactured by Laser Zentrum Hannover e.V., is used for the experiments. This welding head has a four-sided pyramid with a highly reflective coating positioned below a focusing lens. The laser beam is split by the pyramid into four partial beams and deflected outwards. Each partial beam is reflected by a mirror in such a way that all partial beams are recombined in one spot to enable a cladding process. Splitting the laser beam enables wire and media hoses to be inserted into the center of the welding head and thereby enables a coaxial arrangement of both wire and laser beam [24].

The continuous wave diode laser LDM 3000-40, manufactured by Laserline GmbH, with a wavelength range of 1020 to 1060 ± 15 nm, a fiber core diameter of 400 µm and a maximum power output of 3 kW is used as laser source. The collimation unit has a focal length of 100 mm and the focusing unit has a focal length of 300 mm. A focus
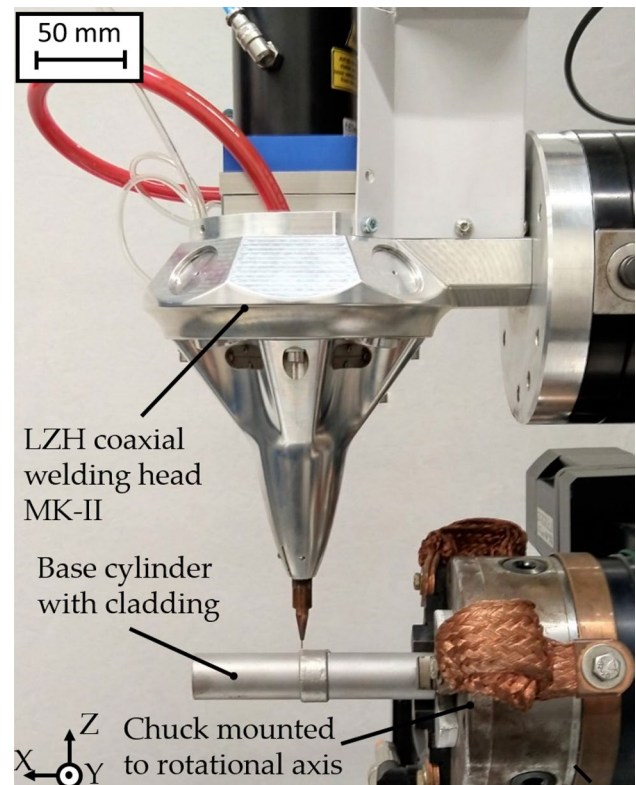
Fig. 3 Experimental setup for laser hot-wire cladding

position of 2.5 mm below the substrate surface is selected for the experiments, resulting in a spot diameter on the workpiece of 3 mm. The wire feed unit DIX FED100 and hot-wire source DIX PI 270, both manufactured by Dinse GmbH, are used for wire feeding and preheating.

Base cylinders with a diameter of 27 mm and a length of 140 mm are used as substrate for the investigations. The base cylinder is clamped in the chuck of a rotary axis. This axis is mounted on the X-Y linear axes. By superimposing rotary motion and linear motion in the axial direction of the shaft, spiral claddings are applied to the base cylinder. The cladding consists of ten adjacent weld seams which are positioned centrally on the base cylinder. A total of two or three cladding layers is applied resulting in an average cladding thickness of 1.9 mm and 2.7 mm. 9 samples of each layer thickness are manufactured. Fig. 4 shows a specimen after LHWC.

An overview of the LHWC process parameters is shown in Table 2.

Fig. 4 Base cylinder with three-layer X45CrSi9-3 cladding

Table 2 Parameters for LHWC of X45CrSi9-3 on 20MnCr5

Parameter	Unit	LHWC
Welding speed	mm/min	1000
Current		
First layer	A	90 A
Following layers	A	80 A
Wire feed rate	m/min	2.0
Laser power	kW	2.1
Shielding gas flow	l/min	6
Wire diameter	mm	1.0
Stickout length	mm	6.9
Seam-to-seam offset	mm	1.6
Laser beam source	–	LDM 3000-40
Laser wavelength range	nm	1020 to 1060 ± 15
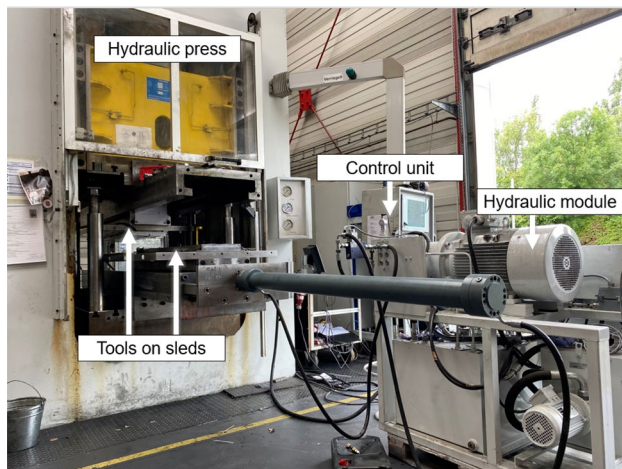
Fig. 5 The CWR module used for hot forming of hybrid workpieces

3.3 Experimental setup for cross-wedge rolling

The hot forming of the hybrid workpieces is performed with a CWR module, which was developed and build by the IPH-Institut für Integrierte Produktion Hannover gGmbH (IPH). The module can be seen in Fig. 5. It consists of two sleds mounted in a hydraulic press. The sleds are moved in the horizontal direction by one hydraulic module each. Vertical movement is realized by the press. The tools for forming the workpieces are attached to the sleds.

Fig. 6 Cross-wedge rolled shaft

The module holds two tools with a length of 1500 mm and a width of 250 mm. During the CWR process, piezo-electric sensors collect information about the contact pressure between the part and the tool at the beginning and at the end of the process. Additionally, thermocouples measure the temperature of the workpiece at critical areas. In this way, temperature information is collected at the start of the rolling process, just before the wedge insertions and at the end of the process.

The tools are preheated to a temperature of 150 °C using cartridges inserted into an aluminum plate at the outer sides of the tools. The workpieces used are 140 mm long and have a diameter of 27 mm. The cladding is applied in the center of the shaft's lateral surface and increases the thickness of the workpiece in this area. To obtain workpieces with a temperature of 1250 °C, an induction heating unit manufactured by EMA-TEC GmbH is used. The heating process takes a total of 60 s. Due to the short heating time, surface decarburization and scale can be minimized. Immediately after heating, the temperature of the workpiece is measured at approximately 1360 °C. After heating the parts are transported and positioned for 20 s before the rolling process starts. The roll gap is set to 28 mm. Once the roll gap is reached, the hydraulic press secures the machine and the tool slides are set in motion and form the workpiece. The forming process takes around 9 s. After rolling, the workpieces are removed and placed either on a steel tray with sufficient air flow or in a water bath for cooling. A rolled shaft is shown in Fig. 6.

3.4 Cladding analysis

After each process step, the cladding properties are analyzed. One sample per parameter set is used to investigate the change of the cladding distribution due to the process steps. Longitudinal cross-sections are made for this purpose. Three shafts for every layer thickness are used to determine the microhardness in the cladding material and in the base material. The position of the microhardness measurement lines in the longitudinal cross-sections is shown in Fig. 7. Six measurement lines are positioned in the cladded area while two measurements lines are positioned on the not cladded part of the shaft as reference. Each measurement line consists of 45 measuring points, each with a spacing of 0.1 mm. The microhardness is measured according to Vickers HV0.1. For each parameter set a mean microhardness will be determined for the measurements in the cladded area
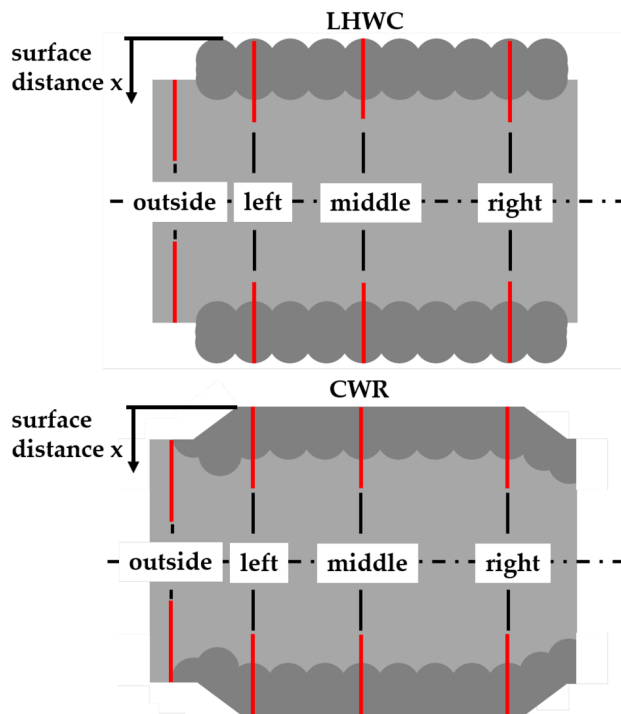
Fig. 7 Position of microhardness measurements in the longitudinal section of the hybrid shaft. Hardness measurement lines in red

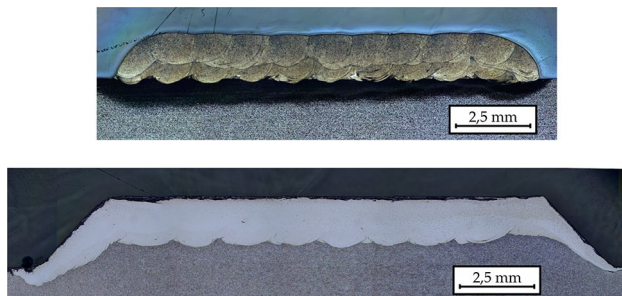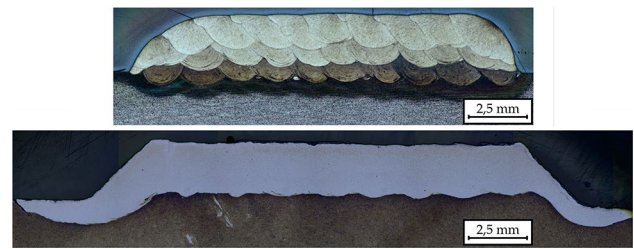**Fig. 9** Cladding layer distribution of a shaft cladded with three layers after LHWC (top) and after CWR (bottom)

distribution cross-sections of the hybrid shafts are examined. After deposition welding the cladding has a mean width of 17.5 mm and the radius of the base cylinder is increased by 1.92 mm (two layers) or 2.74 mm (three layers). Due to the dilution with the base material a maximum cladding thickness of up to 2.28 mm (two layers) or 3.34 mm (three layers) is achieved. After CWR, the approximately 17.5 mm wide bearing seat is completely covered by the cladding. The cladding thickness decreases to 1.93 mm (two layers) and 2.69 mm (three layers), while the cladding width is increased to up to 27.5 mm. The cladding thickness varies due to batch differences caused by the CWR process.

of the shaft and a mean hardness will be determined for the microhardness measurements of the uncladded area of the shaft. In order to investigate the microstructure, cross-sections of samples of each parameter set are made and etched with the etchants Beraha-II and Nital.

4 Results and discussion

4.1 Cladding distribution

The distributions of the claddings after LHWC and CWR are shown in Figs. 8 and 9. For the analysis of the cladding

4.2 Microhardness and microstructure

The mean microhardness values for the bearing seat are calculated from the measurements on the positions left, middle and right as shown in Fig. 7. After LHWC a mean microhardness of 715 HV0.1 is found in the cladding area. The microhardness of the base material is considerably lower at an average of 199 HV0.1. The microhardness in the cladding after the LHWC is significantly higher than in the study on the hybrid bevel gear [20], where only a microhardness of 400 HV0.5 was achieved. The reason for this could be the changed experimental setup (scanner-based with lateral feed vs. coaxial welding head) and the resulting different process speeds and cooling behavior. The microhardness profiles after LHWC of a cladding with two and three layers are shown in Figs. 10 and 11.

The microhardness profiles of the shafts that are cross-wedge rolled and cooled at ambient air are shown in Figs. 12 and 13. A microhardness of 200 to 250 HV0.1 is found in the base material. The microhardness of the cladding varies between 600 and 760 HV0.1. The large fluctuations in microhardness values can be explained in the near-surface area by scale formation and surface decarburization. Different microstructures are present in the cladding, which can lead to fluctuations in the microhardness values, depending on the composition in which they occur in the measuring point.
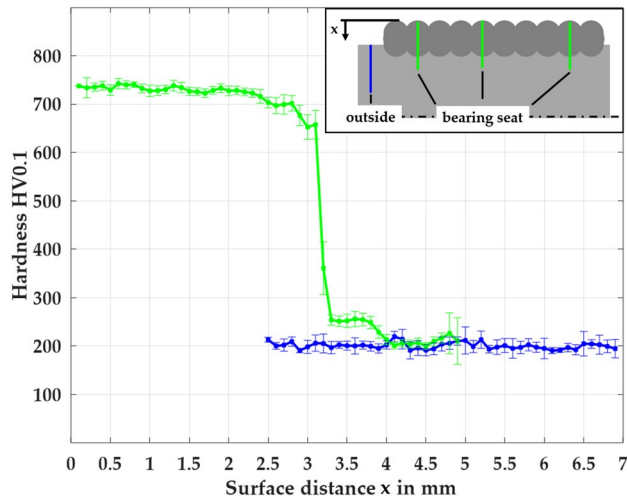

Fig. 8 Cladding layer distribution of a shaft cladded with two layers after LHWC (top) and after CWR (bottom)

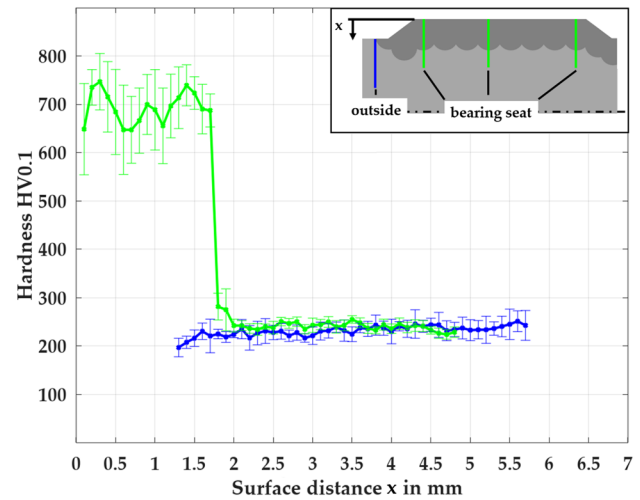**Fig. 10** Microhardness in a two layer cladding after deposition welding

Fig. 12 Microhardness in a two layer cladding cooled in air after cross-wedge rolling
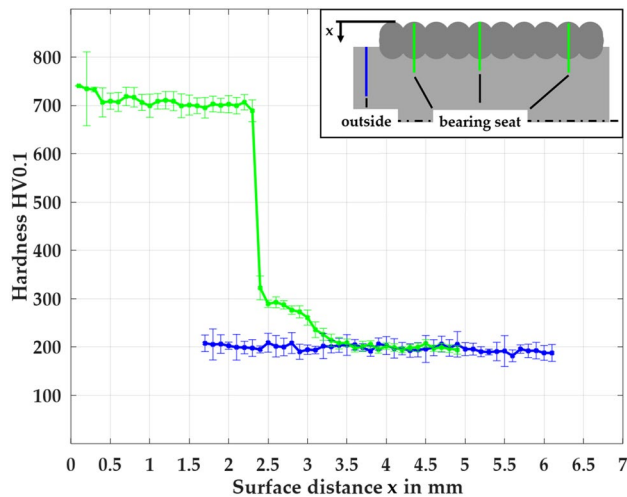

Fig. 11 Microhardness in a three layer cladding after deposition welding
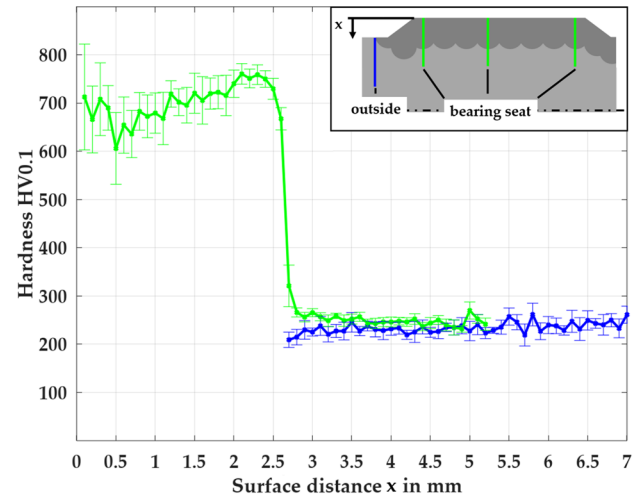

Fig. 13 Microhardness in a three layer cladding cooled in air after cross-wedge rolling

The microhardness of the base material is significantly higher in shafts that are quenched in water after CWR. A microhardness between 450 and 550 HV0.1 is achieved. The microhardness of the cladding is in the range from 680 to 760 HV0.1, which is at the upper end of the microhardness range of the shafts cooled at ambient air. The microhardness values of the air-cooled shafts are subject to greater fluctuations. Therefore the cooling strategy only has a small effect on the microhardness values of the cladding. The microhardness profile of the quenched shafts are shown in Figs. 14 and 15.

The microstructure of the different specimens and layers can be seen in Figs. 16, 17, 18, 19 and 20. For the microstructural examination the images are compared to the

corresponding hardness values in Figs. 10, 11, 12, 13, 14 and 15. Figures 16 shows the microstructure of the transition of the cladding into the base material after LHWC. A martensitic microstructure with retained austenite can be seen in the cladding and a ferritic-pearlitic microstructure in the base material. In Figs. 17 and 19 it can be observed that a martensitic microstructure is formed in the cladding. This is recognizable by the needle-shaped texture of the microstructure and the high hardness values.

The microstructure of the base material depends on the cooling method. Cooling in water leads to a high cooling rate. In Fig. 19 an example for rapid cooling is presented. The cladding has the specific brownish coloration and the base material has a needle-shaped texture that is mainly
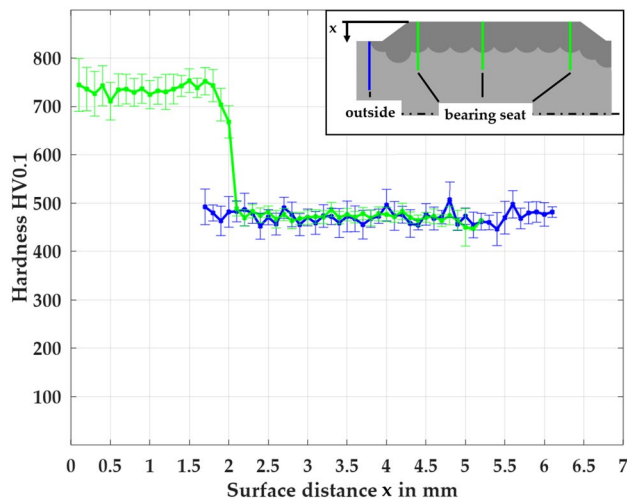
Fig. 14 Microhardness in a two layer cladding quenched in water after cross-wedge rolling
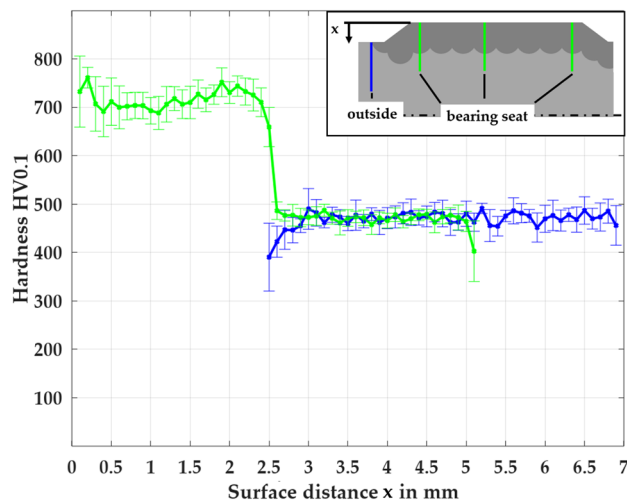

Fig. 16 Microstructure in the transition area from base material to cladding material after LHWC

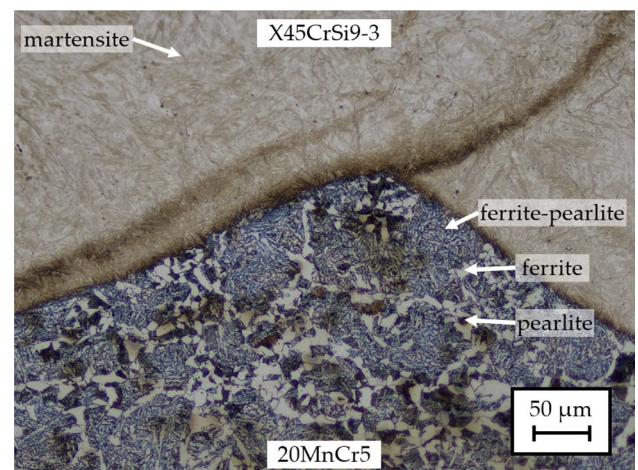**Fig. 15** Microhardness in a three layer cladding quenched in water after cross-wedge rolling

Fig. 17 Microstructure in the transition area from base material to cladding material cooled in ambient air after CWR

blue. Therefore, the microstructure of the base material is identified as mainly martensite. A specimen cooled in air can be seen in Fig. 18. The base material shows grains that have different sizes and no specific shape. The microstructure is mainly white colored with dark colored grain boundaries. It is also visible that some grains are colored darker and some grains have a mixed microstructure with white and blue coloring. In this case, the base material contains mainly ferrite, but also grains of ferrite-pearlite with varying contents of pearlite.

In Fig. 20 it is visible by the changing coloring of the microstructure in the base material that decarburization took place. The closer the structure is to the surface, the more brownish and less bluish it appears. The microstructure appears mostly needle-shaped. Comparing the microstructural results with the corresponding hardness values in Fig. 15 it is concluded that the microstructure mainly contains martensite.

4.3 Mannesmann effect

In Fig. 21 the cross-section of a cladded and cross-wedge rolled workpiece is shown. It is visible that the Mannesmann effect occured and the core has been loosened in the area of the bearing seat. This leads to the formation of voids. The service life of the workpiece is not expected to be reduced by this, since the service life is determined by the material layer on the bearing seat, which is unaffected.
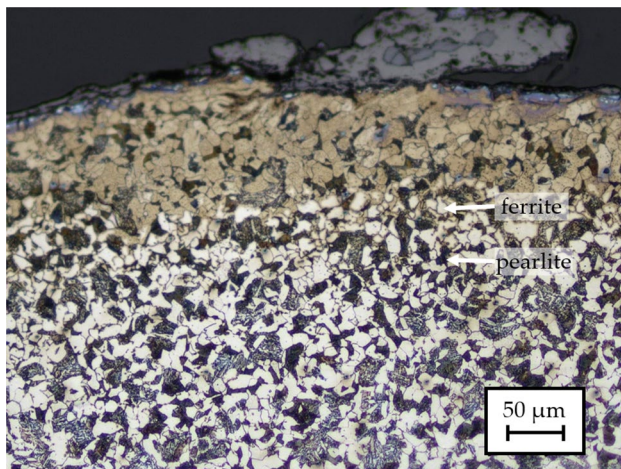
Fig. 18 Microstructure in the base material cooled in ambient air after CWR
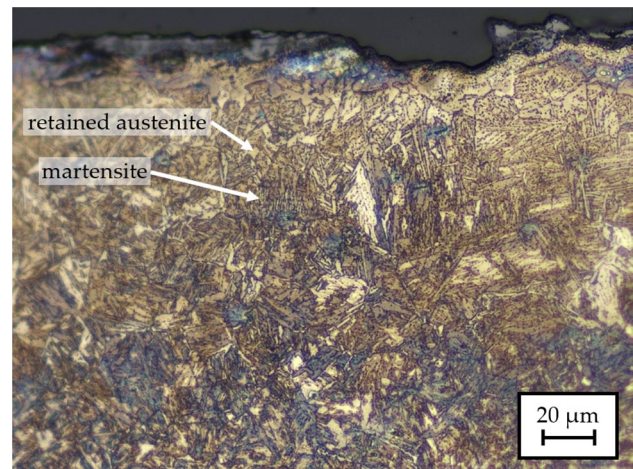

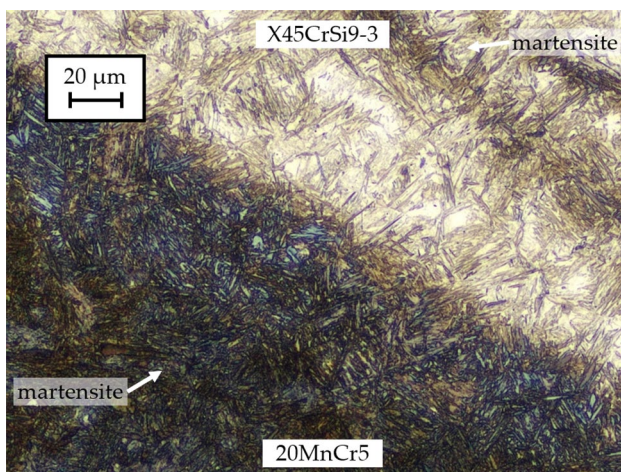**Fig. 20** Microstructure in the base material quenched in water after CWR

Fig. 19 Microstructure in the transition area from base material to cladding material quenched in water after CWR
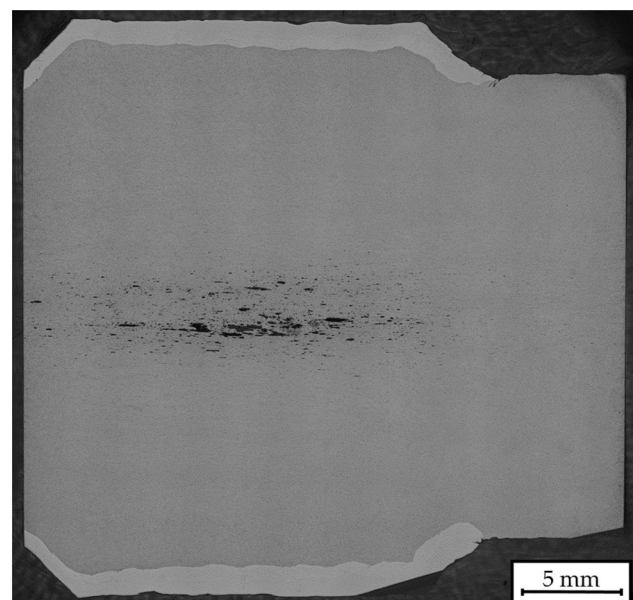

Fig. 21 Mannesmann effect in the base material

All samples examined showed a similar development of this defect, independent of the cladding thickness. It is possible that the application of the cladding increases the stress conditions in the bearing seat, thus leading to void formation during cross-wedge rolling. Using monolithic material the area of the bearing seat has a low probability of void formation due to the low degree of forming in that area. Since the base material has a diameter of 27 mm and the roll gap is set to 28 mm, there is no cross-section reduction. In the case of applied cladding, the thickness of the bearing seat is increased. This leads to it being upset in the beginning of the CWR-process when the upper tool is lowered. The cross-section reduction in the bearing seat according to Pater is 9.1% for cladding with two layers and 14.5% for a cladding with three layers

[12]. Upsetting the bearing seat is necessary and can not be stepped since it increases the degree of forming in the cladding and achieves the necessary forming microstructure. For the combination of 20MnCr5 base material and a cladding made of X45CrSi9-3 the increased cross-section reduction and the combination of two materials with different properties might lead to complex stress conditions that cause internal defects. Possibly, these stress states could be intensified by the formation of manganese sulfide inclusions during forming. Idoyaga et al. researched the effect of sulfur on the Mannesmann effect in rolled steel [25]. The authors found that the material 20MnCr5 is very

susceptible to the Mannesmann effect. 20MnCr5 is a material that is optimized for machining and is therefore used in the Tailored Forming process chain [26].

5 Summary and outlook

In this paper, the Tailored Forming process chain to manufacture shafts with bearing seats made of the material combination X45CrSi9-3 and 20MnCr5 was investigated. The cladded shafts could be formed by cross-wedge rolling without any delamination or cracking of the cladding. However, core loosening due to the Mannesmann effect occurred in the area of the bearing seat, which could reduce the service life under rolling load.

After LHWC a microhardness of 715 HV0.1 was achieved in the cladding, while the microhardness of the base material was significantly lower at 199 HV0.1. The microhardness of the cladding was only slightly affected by the cooling strategy after CWR. A microhardness between 600 and 760 HV0.1 was achieved in the shafts cooled at ambient air, while the cladding of the quenched shafts had a microhardness of 680 to 760 HV0.1 The microhardness of the base material was in the range of 200 to 250 HV0.1 for shafts that were cooled at ambient air. The base material of shafts quenched in water achieved a microhardness of 450 to 550 HV0.1.

Depending on the cooling strategy, different microstructures resulted in the base material. The cladding material, on the other hand, was hardly affected by the cooling. The microstructure in the cladding was martensitic after LHWC. The microstructure of the base material consisted mainly of ferrite and grains of ferrite-pearlite both after LHWC and after CWR and cooling in ambient air. Quenching of the specimens after CWR resulted in a martensitic microstructure.

Since the Mannesmann effect occurred in these studies, future studies should vary the parameters of the cross-wedge rolling process to find a parameter field in which defect-free rolling is possible. Defect-free shafts made of 20MnCr5 and X45CrSi9-3 can be subject to a service life test after machining and heat treatment and compared with shafts made of the material combination C22.8 and X45CrSi9-3. Furthermore, the applicability of other forming processes, such as forging, to the material combination 20MnCr5/X45CrSi9-3 can be investigated. Possible Tailored Forming components would be, for example, bevel gears.

Declarations

References

1. Mildebrath M, Blohm T, Hassel T, Stonis M, Langner J, Maier HJ, Behrens B-A (2017) Influence of cross wedge rolling on the coating quality of plasma-transferred arc deposition welded hybrid steel parts. Int J Emerg Technol Adv Eng 1–7. ISSN 2250_2459

2. Saha MK, Das S (2016) A review on different cladding techniques employed to resist corrosion. J Assoc Eng. https://doi.org/10.22485/jaei/2016/v86/i1-2/119847

3. Kisielewicz A, Pandian KT, Sthen D, Hagqvist P, Bermejo MAV, Sikström F, Ancona A (2021) Hot-wire laser-directed energy deposition: process characteristics and benefits of resistive preheating of the feedstock wire. Metals. https://doi.org/10.3390/met11040634

4. Nowotny S, Brueckner F, Thieme S, Leyens C, Beyer E (2015) High-performance laser cladding with combined energy sources. J Laser Appl 10(2351/1):4817455

5. Kruse J, Mildebrath M, Budde L, Coors T, Faqiri MY, Barroi A, Stonis M, Hassel T, Pape F, Lammers M, Hermsdorf J, Kaierle S, Overmeyer L, Poll G (2020) Numerical simulation and experimental validation of the cladding material distribution of hybrid semi-finished products produced by deposition welding and cross-wedge rolling. Metals 10(10):1336. https://doi.org/10.3390/met10101336

6. Kaierle S, Barroi A, Noelke C, Hermsdorf J, Overmeyer L, Haferkamp H (2012) Review on laser deposition welding: from micro to macro. Phys Proc 39:336–345. https://doi.org/10.1016/j.phpro.2012.10.046

7. Nurminen J, Riihimä J, Näkki J, Vuoristo P (2006) Comparison of laser cladding with powder and hot and cold wire techniques. In: International congress on applications of lasers & electro-optics. http://aip.scitation.org/doi/abs/10.2351/1.5060747

8. Liu S, Liu W, Kovacevic R (2015) Experimental investigation of laser hot-wire cladding. Proc Inst Mech Eng Part B J Eng Manuf 231:1007–1020. https://doi.org/10.1177/0954405415578722

9. Peng W, Jiguo S, Shiqing Z, Gang W (2016) Control of wire transfer behaviors in hot wire laser welding. Int J Adv Manuf Technol 83:2091–2100. https://doi.org/10.1007/s00170-015-7696-8

10. Li Q, Lovell M, Slaughter W, Tagavi K (2002) Investigation of the morphology of internal defects in cross wedge rolling. J Mater

Process Technol 125–126:248–257. https://doi.org/10.1016/S0924-0136(02)00303-5

11. Pater Z, Tomczak J, Bulzak T (2018) New forming possibilities in cross wedge rolling processes. Arch Civ Mech Eng. https://doi.org/10.1016/j.acme.2017.06.005

12. Pater Z (2014) Cross-wedge rolling. Comprehens Mater Process. https://doi.org/10.1016/B978-0-08-096532-1.00315-0

13. Kruse J, Jagodzinski A, Langner J, Stonis M, Behrens B-A (2019) Investigation of the joining zone displacement of cross-wedge rolled serially arranged hybrid parts. Int J Mater Form 13:577–589. https://doi.org/10.1007/s12289-019-01494-3

14. Wang M, Li X, Du F, Zheng Y (2004) Hot deformation of austenite and prediction of microstructure evolution of cross-wedge rolling. Mater Sci Eng A 379:133–140. https://doi.org/10.1016/j.msea.2004.01.055

15. Zhang N, Wang B-Y, Lin J-G (2012) Effect of cross wedge rolling on the microstructure of GH4169 alloy. Int J Miner Metall Mater. https://doi.org/10.1007/s12613-012-0636-9

16. Zhou J, Yu Y, Zeng Q (2014) Analysis and experimental studies of internal voids in multi-wedge cross wedge rolling stepped shaft. Int J Adv Manuf Technol. https://doi.org/10.1007/s00170-014-5768-9

17. Wojcik L, Pater Z, Bulzak T, Tomczak J (2020) Physical modeling of cross wedge rolling limitations. Materials. https://doi.org/10.3390/ma13040867

18. Wójcik L, Pater Z (2019) Physical simulation of the mannesmann effect in the rolling process. Arch Metall Mater 64(4), 1369–1375. https://doi.org/10.24425/amm.2019.130103

19. Silva MLN, Pires GH, Button ST (2011) Damage evolution during cross wedge rolling of steel DIN 38MnSiVS5. Proc Eng. https://doi.org/10.1016/j.proeng.2011.04.125

20. Behrens B-A, Diefenbach J, Chugreeva A, Kahra C, Herbst S, Nürnberger F (2020) Tailored forming of hybrid bevel gears with integrated heat treatment. Proc Manuf 47:301–308. https://doi.org/10.1016/j.promfg.2020.04.234

21. Blohm T, Nothdurft S, Mildebrath M, Ohrdes H, Richter J, Stonis M, Langner J, Springer A, Kaierle S, Hassel T, Wallaschek J, Overmeyer L, Behrens B-A (2017) Investigation of the joining zone of laser welded and cross wedge rolled hybrid parts. Int J Mater Form. https://doi.org/10.1007/s12289-017-1393-0

22. Deutsche Edelstahlwerke Services GmbH (2011) Werkstoffdatenblatt Cr-Mn-legierter Einsatzstahl 1.7147/1.7149 20MnCr5/20MnCrS5. https://www.dew-stahl.com/fileadmin/files/dew-stahl.com/documents/Publikationen/Werkstoffdatenblaetter/Baustahl/1.7147_1.7149_de.pdf. Accessed 16 June 2021

23. Deutsche Edelstahlwerke Services GmbH (2016) Werkstoffdatenblatt X45CrSi9-3 1.4718. https://www.dew-stahl.com/fileadmin/files/dew-stahl.com/documents/Publikationen/Werkstoffdatenblaetter/RSH/1.4718_de.pdf. Accessed 16 June 2021

24. Lammers M, Hermsdorf J, Kaierle S, Ahlers H (2020) Entwicklung von Laser-Systemkomponenten für das koaxiale Laser-Draht-Auftragschweißen von Metall- und Glaswerkstoffen. In: Lachmayer R, Rettschlag K, Kaierle S (eds) Konstruktion für die Additive Fertigung 2019. Springer , Berlin. https://doi.org/10.1007/978-3-662-61149-4_15

25. Idoyaga Z, Elvira R, Wendenbaum J, Meunier J, Robelet M, Toscanelli O, Reis M, Zachäus R, Lorenz B, Kolbe M (2008) Influence of tramp elements (P, Cu, S, Sn) on the Mannesmann effect in the transversal hot rolling of engineering steels (MANNESTRAMP). Technical Steel Research, 23597. European Commission, Report of the Commission of the European Communities—EUR, Brussels

26. Monkova K, Monka PP, Sekerakova A, Tkac J, Bednarik M, Kovac J, Jahatek A (2019) Research on chip shear angle and built-up edge of slow-rate machining EN C45 and EN 16MnCr5 steels. Metals. https://doi.org/10.3390/met9090956